Physical Review B 70 , 2004, 205321-1 –10

Native oxidation of $CuGaSe_2$ crystals and thin films studied by electron paramagnetic resonance and photoelectron spectroscopy

R. Würz[a], A. Meeder[a], D. Fuertes Marrón[a], Th. Schedel-Niedrig[a], A. Knop-Gericke[b], K. Lips[c]

[a]Hahn-Meitner-Institut, Abteilung SE2, Glienicker Strasse 100, D-14109 Berlin, Germany
b Department of Inorganic Chemistry, Fritz-Haber-Institute of the MPG, Faradayweg 4-6, 14195 Berlin, Germany
[c]Hahn-Meitner-Institut, Abteilung SE1, Kekuléstrasse 5, D-12489 Berlin, Germany

Abstract

The oxidation of $CuGaSe_2$ crystals and polycrystalline thin films was investigated with electron paramagnetic resonance (EPR) and photoelectron spectroscopy (PES). An EPR signal assigned to Cu^{2+} evolves when the samples were stored under ambient conditions for a few months, independent of the morphology of the specimens. The formation of a native oxide layer consisting of Ga_2O_3 and SeO_2 was observed in PES during the initial stage of oxidation. Only after long term oxidation for several months an additional copper hydroxide phase, $Cu(OH)_2$, was detected. When the $Cu(OH)_2$ phase was reduced by annealing in vacuum at 200 °C or removed by etching in KCN also the Cu^{2+} EPR signal disappeared. It is shown that the Cu^{2+} EPR signal originates from the $Cu(OH)_2$ phase and the activation energy for the thermal reduction of Cu^{2+} to non-paramagnetic Cu^+ is $E_a = 0.29$ eV. A model for the native oxidation of $CuGaSe_2$ will be presented and implications for solar cell device performance discussed.

I. Introduction and motivation

$CuGaSe_2$ belongs to the class of *I-III-VI*$_2$ semiconducting chalcopyrites. With its high band gap of $E_g = 1.68$ eV at room temperature and optical absorption coefficient larger than 10^4 cm^{-1} for photon energies $h\nu > 1.7$ eV, it is a promising candidate for absorber applications in thin-film solar cells. Up to now energy conversion efficiencies of 9.7% and 9.5% have already been achieved for single-crystal[1] and thin-film cells,[2] respectively. Despite these promising results, these efficiencies are still too low compared to the theoretically predicted value of 26%.[3] Major performance limiting factors are intrinsic and extrinsic defects in the absorber. In particular, it was shown that interface related recombination is enhanced when the *p*-$CuGaSe_2$ thin-film absorber layer is exposed to ambient conditions prior to the deposition of the *n*-CdS emitter.[4] If $Cu(In,Ga)Se_2$ films are exposed to humid air this degradation process is even strongly accelerated.[5]

Electron paramagnetic resonance (EPR) is a powerful tool to identify intrinsic and extrinsic defects of solar cell absorbers. So far defects in $CuInSe_2$ (Refs. 6-10) and $CuGaSe_2$ (Refs. 11-14) have been studied by EPR. In "bulky" powder samples and crystals of $CuGaSe_2$ two extrinsic EPR signals caused by transition metal contamination due to Ni^+ and Fe^{2+} were found.[11,12] A narrow feature at $g \approx 2.003$ was attributed to an intrinsic defect, namely the positively charged selenium vacancy V_{Se}^+.[13,14] A some 100 G broad line at $g = 2.034$ observed in powder samples remained unidentified.[11,12] Another EPR signal was only observed, when $CuGaSe_2$ powder was exposed to air.[11] Its formation was strongly enhanced when the relative humidity of the air was high.[12] The measured g tensor and hyperfine splitting constants were similar to paramagnetic Cu^{2+} defects known in other materials.[15-21] In addition the g tensor of the signal in $CuGaSe_2$ had no axial symmetry ($g_{xx} \neq g_{yy}$).[11,12] Both facts led to the speculation that the aging effect originates from oxidation of non paramagnetic Cu^+ to paramagnetic Cu^{2+} at the surface of the powder samples.[11,12] Since the development of Cu^{2+} signal in powder samples occurred on the same time scale as the degradation of solar cells, Birkholz *et al.*[12] implied, that both processes are associated. However, this proposed oxidation mechanism was neither experimentally verified nor observed for device-grade thin-film material as incorporated in solar cells.

In this paper we study in detail the native oxide formation of $CuGaSe_2$ with EPR and x-ray photoelectron spectroscopy (XPS) on lumps, powder and thin-film samples of $CuGaSe_2$. We observe the formation of a $Cu(OH)_2$ phase

at the surface of thin films with increasing oxidation time that is well correlated with the previously reported EPR signal. Details of the oxidation process as a function of the deposition parameters and the influence of chemical and heat treatments on oxidized samples are presented. The results will be discussed in the framework of a simplified model for oxidation.

II. Experimental

Polycrystalline thin films of $CuGaSe_2$ were grown on Mo coated glass substrates by halogen supported chemical vapor deposition (CVD) in an open tube system. Polycrystalline binary source materials Cu_2Se and Ga_2Se_3 – synthesized from the elements – were subjected to continuous flows of H_2/I_2 and H_2/HCl, respectively, and volatilized due to chemical reactions at a source temperature of 600 °C and at a reactor pressure of 100 mbar. The resulting gases were injected into the substrate zone where they were mixed and cooled down to 500 °C leading to chemical reactions into the solid phase.[22] By adjusting the flow rates the [Ga]/[Cu] ratio of the resulting $Cu_xGa_ySe_2$ films can be controlled.[23] During the growth of the film a $MoSe_2$ interfacial layer forms between the $CuGaSe_2$ film and the Mo layer. The characteristic bent structure of the $MoSe_2$ layer[24] allows us to peel off the $CuGaSe_2$ film from the substrate by adhesive tape (Tesa). By x-ray fluorescence spectrometry (XRF)[24] it was shown, that there are no remnants of Mo on the backside of the peeled-off $CuGaSe_2$ film and no traces of Ga or Cu on the substrate side. Since the adhesive tape is EPR silent, EPR measurements on $CuGaSe_2$ thin films are possible without any disturbing background signals from the substrate. To increase the signal-to-noise ratio the measurable $CuGaSe_2$ volume was enlarged by rolling up the film on the adhesive tape and placing it in an EPR quartz tube. The quartz tube was evacuated to a pressure of $p < 5 \times 10^{-5}$ mbar and then filled with He gas and sealed, to obtain good thermal contact with the cooling gas. For annealing experiments the temperature stability and chemical inertness of the adhesive Tesa tape is not sufficient. For such experiments, the films were peeled off with adhesive kapton tape (polyimid foil). Unfortunately, plain kapton tape reveals an EPR signal at $g = 2.0023$ with a linewidth of $\Delta H_{pp} = 7.4$ G. To obtain the EPR and XPS spectra of as prepared material, these films were transported in Ar atmosphere from the preparation chamber to the EPR and XPS setup to avoid air oxidation. During peeling off and rolling up, the film was exposed to air for about 5 min before evacuating the EPR sample tube. For the XPS measurement the total exposure time to air was about 20 min. Deliberate air oxidation of the films was allowed by storing the films for a certain time under ambient conditions before sealing them in an EPR quartz sample tube. In the following, this natural oxidation procedure is simply called oxidation.

$CuGaSe_2$ powder was prepared from mortared, melt-grown crystals and passed through an 80 µm testing sieve (see Ref. 11). After oxidizing the powder for 56 months it was filled into an EPR quartz tube. A quartz rod was additionally attached inside the quartz tube to compress and fix the powder volume. Finally, the tube was sealed, as described earlier.

In addition, $CuGaSe_2$ lumps consisting of large single crystals were grown by chemical vapor transport in a closed system with iodine as transport agent. For EPR measurements the crystals were fixed inside the EPR quartz tube with spin free glue. Annealing was performed by placing the quartz tube with the sample enclosed in a cylindrical oven, which already had reached the defined temperature. The samples were annealed for 20 min and thereafter immediately removed from the oven to avoid long lasting cooling ramps.

The surface of selected samples was chemically treated in KCN solution (10%) for 3 min. The chemical bath deposition of CdS was performed in a standard CdS bath at 60 °C for 6 min. After KCN and CdS treatment the samples were rinsed in de-ionized water. Details of the samples studied here and the various treatments are listed in Table I.

EPR experiments were performed in a Bruker Elexys 580 spectrometer operating in continuous wave at *X* band microwave frequencies (9.5 GHz) modulating the magnetic field with 100 kHz and using lock-in detection. The modulation amplitude B_{mod} was chosen such that no line distortion of the relevant signals occurred. The microwave power could be varied between $P_{MW} = 0.2$ µW and 200 mW. The samples were cooled in a helium-flow cryostat in the temperature range T = 5 - 300 K. Since the peak-to-peak EPR signal intensity (I_{PP}) obtained on thin films was rather low, background signals originating from the cryostat and the cavity had to be taken into account. A background spectrum taken under identical experimental conditions was always subtracted from the sample spectrum.

XPS measurements were carried out at the BESSY II beamline U49/2 PGM1 with a hemispherical electron analyzer as well as with a commercial XPS setup with Mg K_α as excitation source. At the BESSY II beamline the excitation photon energy was chosen such that the kinetic energy of the photoelectrons was about 300 eV to ensure similar information depths for all spectra. The photon energy was calibrated by measuring the Fermi energy of the sample holder and with help of the known spectrometer work function. Further the C 1s signal from adventitious carbon with a binding energy $E_B = 285.0$ eV was used for energy referencing. The energy resolution of the monochromator was $\Delta E \approx 0.2$ eV. The bulk chemical composition of films was determined by XRF with a Philips MagicsPRO spectrometer and that of crystals by energy dispersive x-ray analysis (EDX) using a Leica/Zeiss LEO430 system with a Röntec M2 detector.

Table I: $CuGaSe_2$ samples used for EPR and XPS measurements, the [Ga]/[Cu] ratio of the films was measured by XRF, that of the crystal by EDX; ox. time means exposure to air under ambient conditions before measurement; "no Cu^{2+}" means no Cu^{2+} signal was detected with EPR or no satellite band was found in the Cu $2p_{3/2}$ spectrum with XPS; sample f0 and f6 stem from the same deposition run.

Sample name	Morpho-logy	[Ga]/[Cu]	EPR ox. time (months)	XPS ox. time (months)	Treatment	Lab name
p1	Powder[a]		56		Annealing, CdS[b]	we06p2
c1	Crystal	0.88 ± 0.14	65		KCN[c]	CGS16
f0	Film	1.079 ± 0.026	0 (no Cu^{2+})			CC891
f1	Film	1.064 ± 0.026	8			02060701
f2	Film	1.045 ± 0.025	17			01090601
f3	Film	1.015 ± 0.024	8			02042401t
f4	Film	1.037 ± 0.025	9		CdS[b]	AB251
f5	Film	1.032 ± 0.025		0 (no Cu^{2+})		AB439
f6	Film	1.079 ± 0.026	2 (no Cu^{2+})	4 (no Cu^{2+}) 10	Annealing	CC889
f7	Film	1.010 ± 0.024	7	7	Annealing	AB94
f8	Film	1.033 ± 0.025	5	16	Annealing	02040801
f9	Film	1.025 ± 0.025		16	KCN[c]	02031303

[a] The powder was prepared by mortaring melt grown crystals.
[b] Standard CdS bath at 60 °C for 6 min.
[c] Etching in KCN solution (10%) for 3 min.

III. Results

A. EPR results

In contrast to bulky samples, a virgin Ga-rich $CuGaSe_2$ film (sample f0) only revealed a small lorentzian-shaped EPR signal at $g = 2.0028(1)$ with a peak-to-peak width of $\Delta H_{pp} = 1.7$ G. The signal is comparable to that observed in unoxidized $CuGaSe_2$ powder.[11,12] Assuming, that the spins are located either at the surface or in the bulk a surface and bulk spin concentration of $2.2 \times 10^8 cm^{-2}$ and $3.3 \times 10^{12} cm^{-3}$ is estimated, respectively. It has a rather low surface and bulk spin concentration of 2.2×10^8 cm^{-2} and 3.3×10^{12} cm^{-3}, respectively. It should be noted that small traces of carbon located at the surface of the film are sufficient to produce a comparable EPR signal.[25] However, after oxidation of films for more than 3 months, a broad isotropic EPR signal develops that is identical to the well-known Cu^{2+} signal found in oxidized powder samples [see Fig. 1(a) and 1(c)]. In contrast to the film, the powder sample reveals an additional signal at $g = 2.338$, which is attributed to Ni^+ coming from contamination of the source materials.[11] Figure 1(b) shows the simulated EPR powder spectrum with a non axial g tensor (the complete set of parameters is listed in Table II). The retrieved parameters

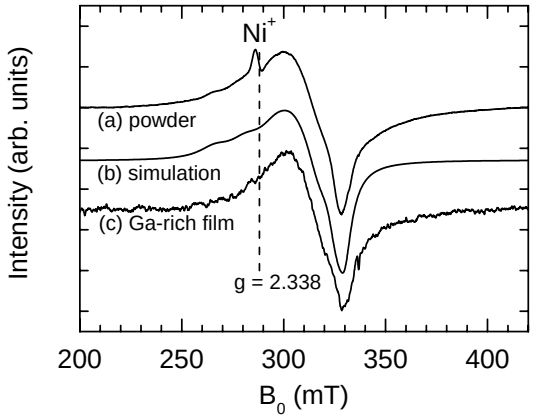

Figure 1: EPR-spectra of oxidized $CuGaSe_2$; (a) powder spectrum (p1), (b) simulated spectrum obtained with the EPR parameters given in Table II, and (c) spectrum of a Ga-rich film (f1, [Ga]/[Cu] = 1.064); all spectra were measured at $T = 6$ K with $P_{MW} = 20$ mW and $B_{mod} = 10$ G at $\nu = 9.44$ GHz.

are nearly identical to those reported by Birkholz *et al.*[11, 12] With decreasing Ga content of the film the line shape of the EPR signal starts to deviate from the powder spectrum. As

shown in Fig. 2(a) a sharp feature at $B_0 = 322.5$ mT evolves.

Table I: Values for the g and A tensor and linewidths l used to simulate the Cu^{2+} signal of the powder [Fig. 1(b)] and the D signal of films [Fig. 2(a)]; both spectra were simulated with $S = 1/2$, $I = 3/2$ and lorentzian line shape.

	Cu^{2+} signal	D signal
g_{xx}	2.07 ± 0.01	2.06 ± 0.005
g_{yy}	2.20 ± 0.01	2.06 ± 0.005
g_{zz}	2.34 ± 0.02	2.34 ± 0.05
A_{xx} / G	15 ± 5	15 ± 5
A_{yy} / G	15 ± 5	15 ± 5
A_{zz} / G	150 ± 10	150 ± 10
l_x / G	35 ± 5	16 ± 2
l_y / G	100 ± 10	16 ± 2
l_z / G	110 ± 10	110 ± 10

This change in line shape is attributed to a second signal, in the following called the D signal. This D signal starts to saturate when the microwave power P_{MW} exceeds 0.1 mW. Since the microwave saturation behavior of the D signal is different from that of the Cu^{2+} signal, it is possible to extract the line shape. For an unsaturated signal the integrated EPR intensity I increases with the square root of P_{MW}, $I \propto P_{MW}^{1/2}$ whereas a signal that is already driven into saturation clearly deviates from this behavior. By comparing the EPR spectrum with both signals unsaturated ($P_{MW} = 0.02$ mW, Fig. 2) with the corresponding spectrum where only the D signal is in saturation ($P_{MW} = 2$ mW), we find that the relative intensity of the D signal has been strongly quenched. By appropriately normalizing the spectrum measured at $P_{MW} = 0.02$ mW with a factor of 10, the difference spectrum reveals the pure D signal around $g_{eff} = 2.0583$ with $\Delta H_{pp} = 90$ G. The D signal is the smaller the higher the Ga content of the film is [Figs. 2(a) and 2(b)]. If this procedure is carried out on the powder sample [Fig. 2(c)] no difference signal is found. The D signal reveals a pronounced hyperfine structure. We can simulate the D signal with similar line parameters and g tensor as for the Cu^{2+} signal (see Table II), but with axial symmetry ($g_{xx} = g_{yy}$). This important observation implies that the D center has the same microscopic origin as the Cu^{2+} center and only the crystallites where these centers are located have a preferential orientation. This explanation is supported by texture measurements with x-ray diffraction. CVD grown thin films show a preferential orientation of crystallites towards the <221>-direction.[26] This (112)-texture increases with decreasing Ga content, reaching its maximum at stoichiometric film composition, the same dependence as observed for the D signal. It seems that this change in symmetry induced by the variation in Ga content leads to the observed difference in saturation behavior.

Since it became obvious from the results in Fig. 1 that the Cu^{2+} signal observed in both, powder samples and films, is coupled with oxidation of $CuGaSe_2$, the microscopic origin of the signal is expected to be located at the near-surface region of the $CuGaSe_2$ crystallites. To verify this experimentally, we have etched an oxidized $CuGaSe_2$ crystal (sample c1) in KCN solution (10%) for 3 min. From literature it is known, that KCN etching removes copper selenide phases[27] as well as oxide phases[28] from the surface of chalcopyrite films. Figure 3 compares the

Figure 2:. EPR spectra measured at two different microwave intensities for (a) a stoichiometric film (f3, [Ga]/[Cu] = 1.015),

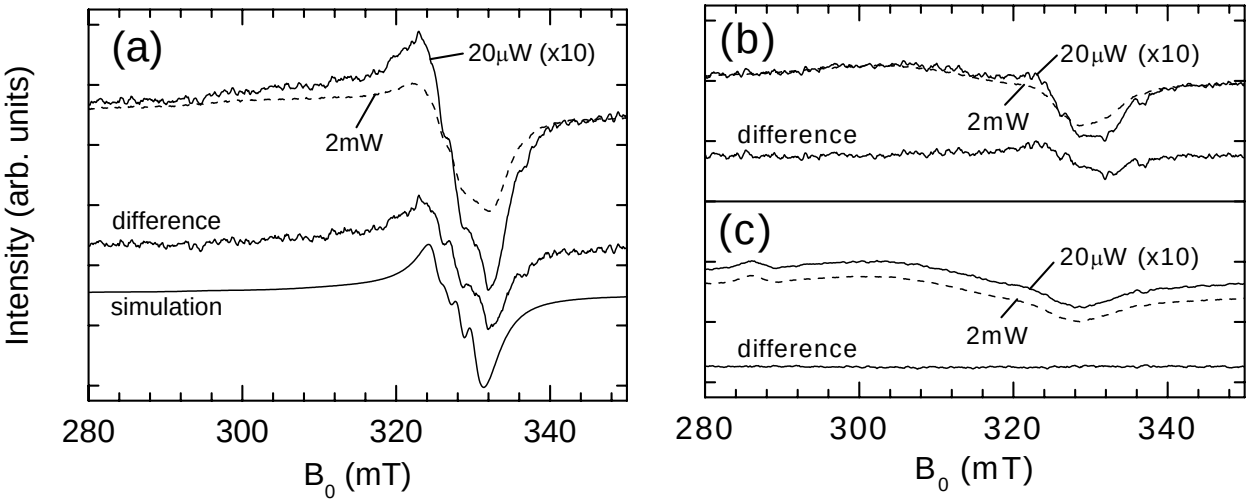

(b) a Ga-rich film (f2, [Ga]/[Cu] = 1.045), and (c) powder (p1). The spectra measured at 20 μW are scaled by a factor of 10 to compensate for the smaller signal response. In addition the difference spectra are plotted. The spectra were normalized so that the spectra measured at 2 mW all have the same intensity at $B_0 = 302.5$ mT. All spectra were measured at $T = 6$ K with $B_{mod} = 10$ G at $\nu = 9.45$ GHz.

EPR spectra before and after KCN etching. The KCN treatment has decreased the peak to peak intensity of the Cu^{2+} signal of the crystal by 86%. Note that the small Ni^+ signal which stems from the bulk of the crystal, remains unchanged after etching. This result gives strong proof, that the Cu^{2+} signal stems from a surface-near layer.

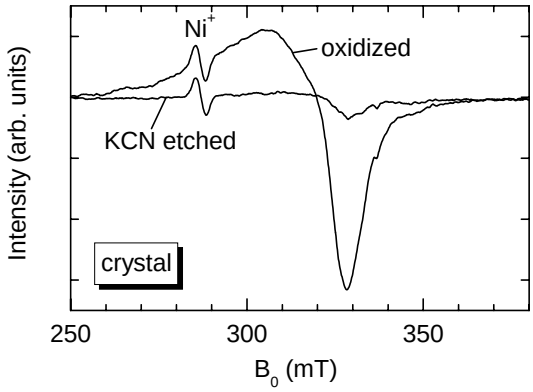

Figure 3: EPR spectrum of an oxidized $CuGaSe_2$ crystal (c1) before and after KCN etching; measured at $T = 6$ K with $P_{MW} = 20$ mW and $B_{mod} = 10$ G at $\nu = 9.45$ GHz.

Unfortunately, KCN etching of the thin films was hard to realize, since in most cases they peeled off from the Mo coated glass substrates during etching. Films which remained on the substrate during KCN etching could no longer be peeled off with the procedure described above. Therefore surface treatment of thin films was done in a CdS bath. This chemical process is used for the emitter deposition of solar cells and is known to etch the oxide phases at the surface of $Cu(In,Ga)Se_2$ absorber layers as well.[29] For this, half of the thin-film (sample f4) was peeled off from the substrate and sealed in an EPR tube to serve as a reference for the untreated surface. The second, equally large part of the sample was treated in the chemical bath and then also peeled off and sealed in the quartz tube. Figure 4(a) shows that the Cu^{2+} signal completely vanishes after the CdS treatment. For comparison, we also treated a powder sample (p1) in the chemical bath. The powder was strewn on adhesive kapton tape and immersed in the CdS bath. A pure powder spectrum without kapton foil was used as untreated reference, since it was impossible to measure EPR at the same specimen on kapton foil before and after the CdS treatment. Both spectra were normalized to the same bulk Ni^+ signal intensity, which was shown not to change with surface treatment. As can be seen in Fig. 4(b) also for the powder samples the CdS bath strongly quenches the Cu^{2+} signal.

As the Cu^{2+} signal was shown to be a surface related signal, we can determine the surface spin density N_{surf} by comparing the EPR signal intensity with a calibrated spin standard. For the powder p1 we estimate a concentration of $N_{surf} \approx (1.1 \pm 0.4) \times 10^{14}$ cm^{-2}, for the film f1 we obtain $N_{surf} \approx (4.1 \pm 1.3) \times 10^{14}$ cm^{-2} assuming a flat film surface or $N_{surf} \approx (1.4 \pm 0.4) \times 10^{14}$ cm^{-2} assuming tetrahedral crystallites increasing the surface by a factor of three. These values are slightly lower than the nominal surface concentration of Cu atoms of 7.3×10^{14} cm^{-2} at {112} planes.

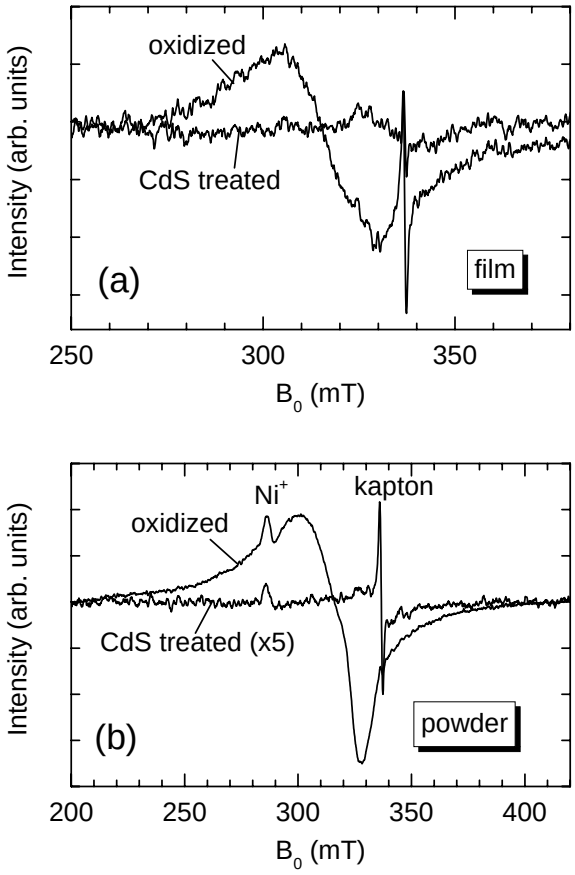

Figure 4: EPR spectra of oxidized $CuGaSe_2$ before and after chemical bath deposition of CdS for (a) a film (f4) and (b) powder (p1). For CdS treatment the powder was strewn on kapton foil. All spectra were measured at $T = 6$ K with $B_{mod} = 10$ G at $\nu = 9.44$ GHz. Spectra in (a) and (b) were measured with $P_{MW} = 20$ and 2mW, respectively.

Since it is well known that an additional heat treatment after the CdS deposition helps to further improve solar cell efficiency,[30] the question remains to what extent the Cu^{2+} can be reduced by annealing. After annealing thin films in He atmosphere or air at 200 °C for 30 min, the Cu^{2+} signal completely vanishes (not shown here). This means that Cu^{2+} has been reduced into non paramagnetic Cu^+. The determination of the activation energy of this reduction process was only possible with the $CuGaSe_2$ powder sample p1 due to sensitivity factors. With stepwise annealing the Cu^{2+} signal strongly reduces until it completely vanishes at an annealing temperature $T_A = 280$ °C (Fig. 5). Note that the signal intensity of the Ni^+ stemming from the bulk of the crystallites remains unchanged. The reduction process of the Cu^{2+} signal in the powder is temperature activated as is shown in Fig. 5(b). For simplicity, the peak-to-peak intensity I_{PP} is plotted since the linewidth of the Cu^{2+} signal did not change with annealing. The Cu^{2+} signal intensity strongly decreases above $T_A = 80$ °C.

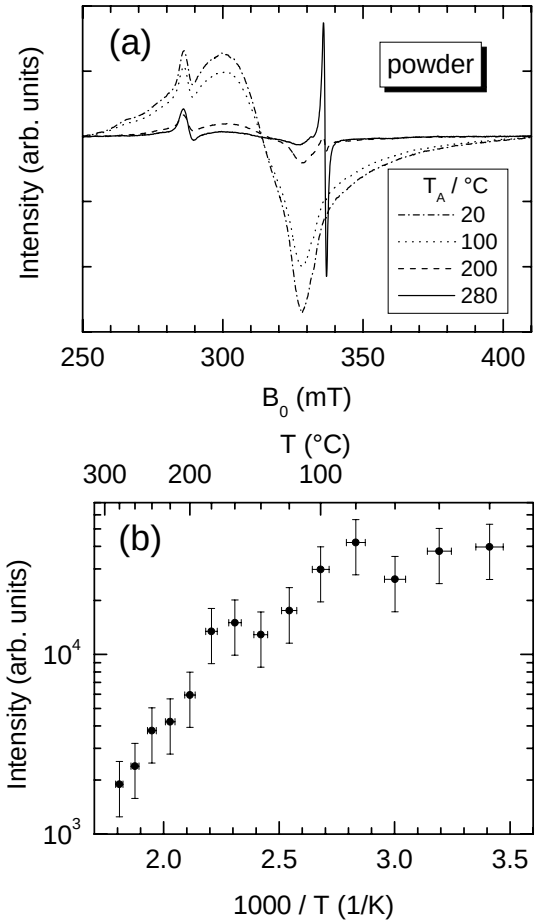

Figure 5: (a) EPR spectra of oxidized $CuGaSe_2$ powder after stepwise annealing at different temperatures in He atmosphere, measured at $T = 6$ K with $P_{MW} = 20$ mW and $B_{mod} = 10$ G at $\nu = 9.44$ GHz, (b) Arrhenius plot of the peak to peak intensity of the Cu^{2+} signal from (a).

In both, films and powder samples, for $T_A \geq 140$ °C a narrow EPR signal at $g = 2.0035 \pm 0.0002$ evolved [Fig. 5(a), $B_0 = 337$ mT]. The linewidth of this signal depends on T_A and is found to decrease from $\Delta H_{pp} = 7.0$ G at $T_A = 280$° C to $\Delta H_{pp} = 5.7$ G and $\Delta H_{pp} = 4.9$ G at $T_A = 360$ °C and 500 °C, respectively, which is accompanied by a further increase in signal intensity. After annealing at 500 °C the spin concentration of this signal was estimated to $N_{surf} = (9.5 \pm 3.0) \times 10^{12}$ cm^{-2} for a surface and $N_{bulk} = (7.1 \pm 2.3) \times 10^{15}$ cm^{-3} for a bulk related signal. Nishi *et al.*[13] found a similar signal in $CuGaSe_2$ when they annealed their samples and assigned the EPR line to a positively charged Se vacancy V_{Se}^{+}.[13] In binary compounds, the anion vacancy has similar line parameters, for instance in ZnSe epilayers the V_{Se}^{+} signal is found at $g = 2.0027$ with $\Delta H_{pp} = 5.8$ G.[31] Also in ternary compounds like $CuInSe_2$ a signal at $g = 2.0030$ with $\Delta H_{pp} = 5$ G evolves upon annealing.[9] Although there is a strong similarity with respect to the EPR signal at $g \approx 2.003$ upon annealing, it should be emphasized that also small contaminants of hydrocarbons appear in EPR spectra at the same g value when annealed above 100 °C.[25] At this stage, no direct spectroscopic evidence is available that, indeed, the line at $g \approx 2.003$ is related to a selenium vacancy.

B. Photoelectron spectroscopy

The KCN and CdS treatments on oxidized crystals and films (Figs. 3 and 4) proved that the Cu^{2+} signal is related to paramagnetic copper in a near-surface region. To obtain information on (i) the chemical bonding state of Cu^{2+} and (ii) the reduction reaction pathway to non paramagnetic Cu^{+}, we have studied the oxidation process by using surface sensitive photoelectron spectroscopy (PES). The Cu $2p_{3/2}$ spectra of thin films oxidized for different times are plotted in Fig. 6. The as prepared film reveals the typical Cu $2p_{3/2}$ peak of $CuGaSe_2$ with a binding energy $E_B = 932.2$ eV.[32] After oxidation for 4 months a shift of the line to $E_B = 932.6$ eV is observed. A shift of the Cu $2p_{3/2}$ peak to higher binding energies was also found after thermal oxidation of $CuInSe_2$ and was attributed to the formation of a $Cu_{2-x}Se$ phase.[33] With further oxidation time a second structure appears at $E_B = 934.8$ eV connected with a satellite band that consists of two lines at $E_B \approx 941$ and 944 eV. These satellite peaks are a characteristic feature for paramagnetic Cu^{2+} (Ref. 34) and give strong support to the interpretation of the EPR data.

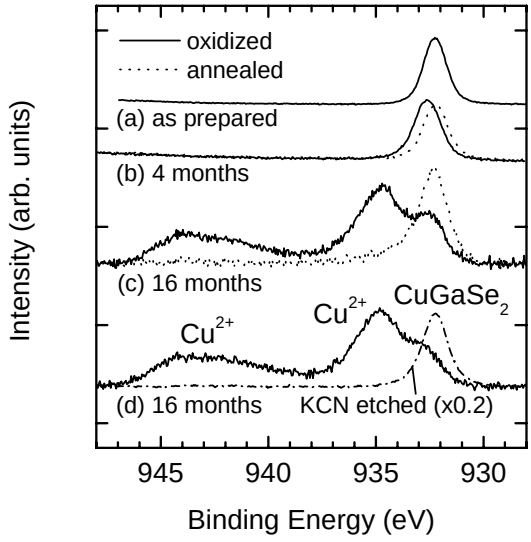

Figure 6: Cu $2p_{3/2}$ spectra of $CuGaSe_2$ films after oxidation (solid curves), after vacuum annealing at 200 °C (dotted curves) and after KCN etching (dash dotted curve), (a) f5 as prepared, (b) f6 after 4 months, (c) f8 after 16 months, and (d) f9 after 16 months oxidation. Spectra in (a) and (b) were acquired with monochromatized synchrotron radiation ($h\nu = 1234$ eV), spectra in (c) and (d) with Mg K_α radiation ($h\nu = 1253.6$ eV).

Table III. XPS binding energy for the Cu $2p_{3/2}$ peak, its satellite band, difference of both and kinetic energy of the Cu *LVV* Auger peak given in electron-volts (with uncertainty ±0.2 eV) measured at oxidized $CuGaSe_2$ samples compared to literature data for $Cu(OH)_2$, CuO, Cu_2O, Cu^0, and $CuGaSe_2$

sample	Cu $2p_{3/2}$	satellite band		difference		Cu(LVV)
f7	934.3	940.9	943.6	6.6	9.3	916.8[a]
f8	934.8	940.9	943.9	6.1	9.1	917.2[a]
f9	934.8	941.1	944.0	6.3	9.2	917.1[a]
$Cu(OH)_2$	934.4[b]	940.6[b]	943.4[b]	6.2[b]	9.0[b]	
CuO	933.8[b]	941.6[b]	944.0[b]	7.8[b]	10.2[b]	918.2[c]
	933.5[d]					917.9[d]
Cu_2O	932.5[b]					916.7[c]
	932.2[d]					917.4[d]
Cu^0	932.5[b]					919.0[c]
	932.4[d]					918.6[d]
$CuGaSe_2$	932.2[e]					917.0[f]

[a]After vacuum annealing at 200 °C, [b]Reference 35, [c]Reference 36, [d]Reference 37, [e]Reference 32, [f]Reference 38.

Since XPS is extremely sensitive to small changes in the local binding configuration, it is possible to distinguish between the various Cu oxidation products that might exist after oxidation (see Table III). For instance, the Cu $2p_{3/2}$ peak of $Cu(OH)_2$ is shifted in comparison to CuO by about 0.6 eV to higher binding energy,[35] which can be reliably detected in the XPS spectra. From the analysis of the spectra as plotted in Table III, we find that the experimentally determined values for the binding energy of the Cu $2p_{3/2}$ line are in better agreement with what has been reported for $Cu(OH)_2$ rather than for CuO, in particular with regard to the distance of the satellite peaks to the Cu $2p_{3/2}$ peak. From this observation we propose, that oxidation of copper at the surface of $CuGaSe_2$ films results in a $Cu(OH)_2$ phase. The oxy-hydride involved can explain the aging process observed in EPR,[12] which is accelerated when oxidizing under humid condition.

Annealing the film in vacuum at $T_A = 200$ °C [Fig. 6(c)] or etching in KCN solution [Fig. 6(d)] completely removes the $Cu(OH)_2$ features and restores the Cu $2p_{3/2}$ line of $CuGaSe_2$ at $E_B = 932.2$ eV as was observed on the virgin sample. This proves that annealing reduces Cu^{2+} to Cu^+ and KCN removes the Cu^{2+}.

To gain further insight into the oxidation and reduction mechanism of Cu at the surface of $CuGaSe_2$, we have also studied the Ga 3*d* spectra of the films f5, f6, and f8 (Fig. 7). Whereas the virgin film exhibits only the typical Ga 3*d* peak of $CuGaSe_2$ with a binding energy $E_B = 19.4$ eV,[32] a shift of the line to $E_B = 20.1$ eV is observed after oxidation. This is indicative of Ga_2O_3 in the near-surface region ($E_B = 20.4$ eV).[39] The Ga $L_3M_{45}M_{45}$ Auger spectra (not shown here) also support the formation of Ga_2O_3. After annealing the films in vacuum at 200 °C the Ga 3*d* spectra could not be restored to the virgin case. Instead, we observe an increase in intensity of all lines (dotted curves in Fig. 7). The difference spectrum [dashed curve in Fig. 7(b)] reveals, that here only the $CuGaSe_2$ related peak increased in intensity. KCN etching [Fig. 7(d)] removes the Ga_2O_3 related features.[40]

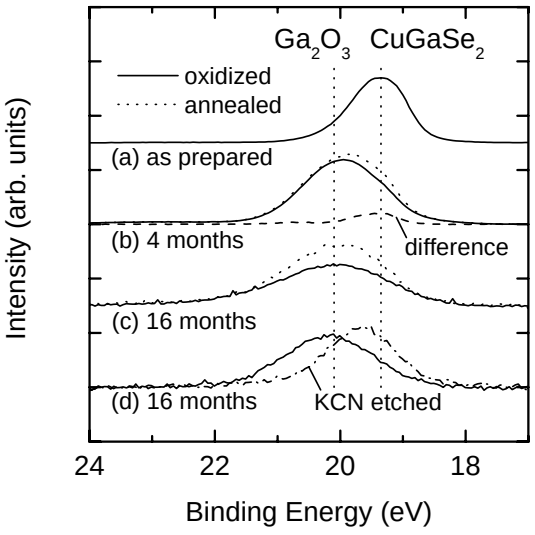

Figure 7: Ga 3*d* spectra of $CuGaSe_2$ films after oxidation (solid curves), after vacuum annealing at 200 °C (dotted curves) and after KCN etching (dash dotted curve), (a) f5 as prepared, (b) f6 after 4 months, (c) f8 after 16 months, and (d) f9 after 16 months oxidation. Spectra in (a) and (b) were acquired with monochromatized synchrotron radiation ($h\nu = 318$ eV), spectra in (c) and (d) with Mg K_α radiation ($h\nu = 1253.6$ eV).

The oxidation process also involves Se as can be seen from the Se 3*d* spectra of the films (solid curves in Fig. 8). The PE spectrum of the virgin sample consists of the well known Se 3*d* doublet structure [Fig. 8(a)] that ex

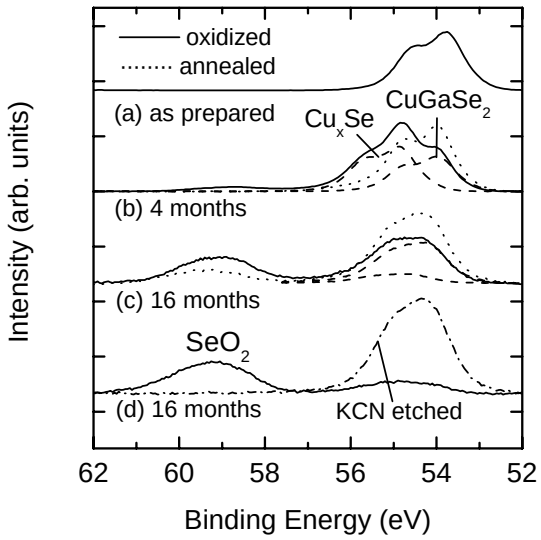

Figure 8: Se 3*d* spectra of $CuGaSe_2$ films after oxidation (solid curves), after vacuum annealing at 200 °C (dotted curves) and after KCN etching (dash dotted curve), (a) f5 as prepared, (b) f6 after 4 months, (c) f8 after 16 months, and (d) f9 after 16 months oxidation. The dashed curves show the components used to fit the oxidized spectra. Spectra in (a) and (b) were acquired with monochromatized synchrotron radiation (hν = 354 eV), spectra in (c) and (d) with Mg K_α radiation (hν = 1253.6 eV).

ists due to the spin-orbit splitting of the 3*d* electrons into a $3d_{5/2}$ (E_B = 53.9 eV) and a $3d_{3/2}$ level (E_B = 54.8 eV). After an oxidation time of 4 months a peak at E_B = 58.8 eV arises that increases with increasing oxidation time and can be assigned to SeO_2.[41] Simultaneously, the Se 3*d* peak has broadened and can be fitted by two sets of doublets, namely the two Se 3*d* lines from the $CuGaSe_2$ phase as well as by a second doublet with $E_B(3d_{5/2}/3d_{3/2})$ = 54.8 / 55.7 eV. This second doublet structure is interpreted to originate from the formation of a $Cu_{2-x}Se$ phase. For $CuInSe_2$ it is well known, that a $Cu_{2-x}Se$ phase forms at the interface between a binary In_2O_3 oxide phase and the ternary chalcopyrite bulk phase.[33] Kazmerski *et al.*[33] found, that the Cu $2p_{3/2}$ and Se 3*d* binding energy for the $Cu_{2-x}Se$ phase were shifted by 0.6 and 0.7 eV to higher values compared to $CuInSe_2$, respectively. Similar shifts for copper selenide compared to $CuInSe_2$ were also found by other groups.[42,43]

Annealing in vacuum results in a strong change of the Se 3*d* spectra (dotted curves in Fig. 8). For the thin film that was oxidized for 4 months [Fig. 8(b)] the SeO_2 related peak at E_B = 58.8 eV vanishes, while for the film oxidized for 16 months [Fig. 8(c)] it only decreases. Simultaneously, the intensity of the doublet with $E_B(3d_{5/2})$ = 53.9 eV related to $CuGaSe_2$ increases, whereas the doublet with $E_B(3d_{5/2})$ = 54.8 eV related to $Cu_{2-x}Se$ disappears. KCN etching of a film oxidized for 16 months [Fig. 8(d)] shows similar effects like annealing but completely removes the SeO_2 phase.

To summarize this section, we have shown that during a 4 month air oxidation process binary oxides, predominantly Ga_2O_3 and some amount of SeO_2, and $Cu_{2-x}Se$ form, whereas we did not find formation of a copper oxide phase. Only after oxidation for longer than 4 months we were able to detect $Cu(OH)_2$ in the near-surface region. After thermal treatment in vacuum at 200 °C the $Cu(OH)_2$, SeO_2, and $Cu_{2-x}Se$ related features in the XPS spectra vanish, while the characteristics of Ga_2O_3 remain. Etching of the oxidized film surface in KCN solution removes all oxide phases.

IV. Discussion

The combination of complementary techniques such as EPR and PES reveals that the storage of pristine $CuGaSe_2$ ternary compound semiconductor under ambient conditions leads to the growth of a native oxide layer. The EPR results show that in all thin-film samples irrespective of their Ga content paramagnetic Cu^{2+} is identified only after an oxidation time longer than 4 months (Table I). Both annealing [Fig. 5(a)] and chemical treatments like KCN etching (Fig. 3) or chemical deposition of CdS [Fig. 4(b)] leave the Ni^+ signal from the bulk of the samples unchanged, whereas the Cu^{2+} signal vanishes. Hence, the Cu^{2+} EPR signal is assigned to Cu^{2+} ions located in the surface/near-surface region. Photoemission results reveal formation of a $Cu(OH)_2$ phase showing a satellite feature in the Cu $2p_{3/2}$ spectrum characteristic for paramagnetic Cu^{2+} only after long term oxidation. The $Cu(OH)_2$ related features in the Cu $2p_{3/2}$ spectrum also vanish after vacuum annealing [Fig. 6(c)] and after KCN etching [Fig. 6(d)]. This strong correlation between EPR and photoemission results suggests that $Cu(OH)_2$ formed in the course of long term oxidation process is the origin for the Cu^{2+} EPR signal.

Generally, the driving force for the growth of native oxide layers on metal and semiconductor solid state surfaces is the minimization of the surface free-energy of the system, since the surface free-energies of oxides are much lower than for the metals or semiconductors. Thus, metals and semiconductors are always covered by a substance which lowers the surface free- energy of the system. Usually, they are covered by ultrathin layers of hydrocarbons, oxides often also by water (OH groups).[44]

According to the photoemission results we propose a simple model for the oxidation of $CuGaSe_2$ as illustrated in Fig. 9. The surface of the as prepared thin film shows a copper-depleted surface composition of about $CuGa_3Se_5$ [Fig. 9(a) and Ref. 32]. The native oxidation starts with the growth of the thermodynamically most stable Ga_2O_3 (see Table IV). The remaining Cu and Se readjust at the interface to form an interfacial $Cu_{2-x}Se$ layer. Addition

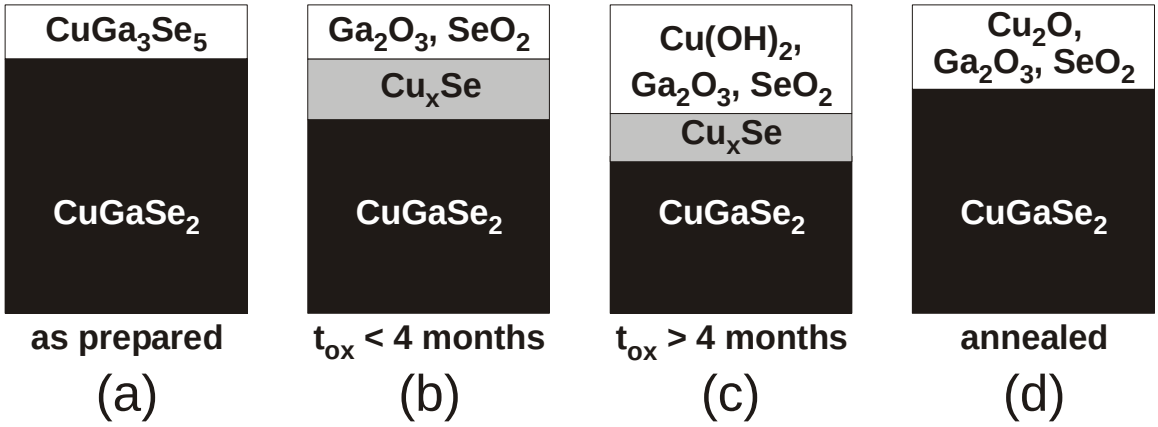

Figure 9: Model for the native oxidation of $CuGaSe_2$ in air under ambient conditions (a) as prepared, (b) after short term oxidation (t_{ox} < 4 months), (c) after long term oxidation (t_{ox} > 4 months), and (d) after annealing of (c) at 200 °C.

Table IV: Standard molar enthalpy (heat) of formation $\Delta_f H^0$ at 298.15 K in kJ/mol of different compounds[45,46]

compound	Ga_2O_3	$Cu(OH)_2$	SeO_2	Cu_2O	CuO	Cu_2Se	CuSe
$\Delta_f H^0$	-1089.1	-449.8	-225.4	-168.6	-157.3	-65.26	-39.5

ally, SeO_2 is formed consuming the excess Se. During a "long term" oxidation process of more than 4 months the amount of this SeO_2 phase increases [Fig. 9(c)] and $Cu^{2+}(OH^-)_2$ is formed as third oxide phase. The small Cu^+ ions of the bulk diffuse from the Cu_xSe/oxide or $CuGaSe_2$/oxide interface towards the surface of the native oxide layer consisting of Ga_2O_3 and SeO_2. This copper transport through the oxide layer is mediated via cationic vacancies either inside the bulk of the native oxide layer or in the grain boundaries.[47] At the surface of the native oxide the Cu^+ ions react with the hydroxyl groups of the adsorbed water to form an outwardly growing $Cu^{2+}(OH^-)_2$ layer. This explains why humid air accelerates the growth of the Cu^{2+} EPR signal.[12] Further, it is in accordance with the results of Cano *et al.*[48] who found that the $Cu(OH)_2$ content in the native oxide layer covering pure Cu metal surfaces increases with an enhanced relative humidity.

According to the order of standard molar enthalpy (heat) of formations (see Table IV) one would expect that the growth of $Cu(OH)_2$ already occurs after short term oxidation before SeO_2 is formed, which was not observed here for the thin films. The Cu depletion of as grown film surfaces accompanied by a Se rich surface composition favors the growth of SeO_2 instead of $Cu(OH)_2$. Powder samples show the formation of Cu^{2+} already after 16 days,[12] whereas in thin films it was only detected after more than 4 months. The different oxide growth rates can be explained by a lower concentration of surface Cu atoms for films in contrast to powder samples. The concentration of surface Cu atoms for the crystallites of the powder sample is expected to be equal to the stoichiometric bulk value of $CuGaSe_2$ instead of $CuGa_3Se_5$ for thin films.[32] Additionally, the permeability of the reactive gas species like oxygen and water molecules is higher in the powder accelerating an oxide growth process for the polycrystalline powders.

Thermal reduction of the long term oxidized films and powder samples in He atmosphere or in air was found to decrease the Cu^{2+} EPR signal which is strongly supported by photoemission experiments. The corresponding thermal reduction procedure performed on thin films removes the satellite peaks in the Cu $2p_{3/2}$ spectrum, which are characteristic for Cu^{2+}. Thus, the paramagnetic surface-/near surface Cu^{2+} ions are transformed into non paramagnetic Cu^+ ions. We therefore propose the thermal reduction of paramagnetic $Cu(OH)_2$ into non paramagnetic Cu_2O at the film surface according to the reaction

$$2\ Cu(OH)_2 \rightarrow Cu_2O + 2\ H_2O + 1/2\ O_2. \qquad (1)$$

A direct proof for the formation of Cu_2O cannot be given by the XPS spectra, as Cu_2O is hard to distinguish from $CuGaSe_2$ by XPS (see Table III). The Cu *LVV* Auger peak of the annealed samples can be attributed to CuO_2 as well as to $CuGaSe_2$. Further, after vacuum annealing at 200 °C the interfacial $Cu_{2-x}Se$ layer vanishes and the amount of SeO_2 at the surface decreases [Fig. 9(d)]. This can be explained by sublimation of SeO_2 from the solid state phase as the vapor pressure at 200 °C is higher than 1 mbar.[45] Hence, the thickness of the native oxide layer decreases [Fig. 9(d)] and all $CuGaSe_2$ related features in the XPS spectra increase.

It is assumed, that the reduction reaction (1) is of second order type, as the concentration of $Cu(OH)_2$ is twofold in Eq. (1). In this case the intensity of the Cu^{2+} EPR signal $I(t)$, which is proportional to the of amount of $Cu(OH)_2$, remaining after an annealing time t at the temperature T_A is given by

$$1/I(t) = 1/I(t = 0) + K \cdot t. \qquad (2)$$

Here $I(t = 0)$ is the EPR signal intensity when starting the annealing at T_A and K is the thermally activated reaction constant K given by

$$K = K_0 \cdot \exp(-E_a/k_B T_A), \qquad (3)$$

with the activation energy E_a and the Boltzmann factor k_B. The reaction constant K for each annealing temperature T_A can be calculated with Eq. (2), as we have measured the EPR signal intensity $I(t = 0$ min) and $I(t = 20$ min) before and after annealing for $t = 20$ min. By an Arrhenius plot of K an activation energy of $E_a = 0.29 \pm 0.09$ eV was determined for the reduction reaction (1). This value is in the range of the activation energy for oxidation of copper in dry and wet oxygen (15% H_2O in O_2) of 0.68 and 0.43 eV, respectively.[49] The corresponding value for the reduction reaction is expected to be lower in the presence of adsorbed carbon, as carbon decreases the reduction temperature of copper oxides.[50,51]

According to our model the thermal reduction only affects the Cu^{2+} EPR signal in the surface /near-surface region, whereas the Ni^+ EPR signal from the bulk remains unchanged (Fig. 5). The same is found after the KCN etching (Fig. 3) or the CdS bath [Fig. 4(b)], where the complete $Cu(OH)_2$ layer is removed. The upper limit for the thickness of the $Cu(OH)_2$ layer containing the paramagnetic Cu^{2+} ions is the thickness of the entire native oxide layer, as it is completely removed by KCN etching. From the increase in intensity of the $CuGaSe_2$ related peak ($E_B = 932.2$ eV) in the Cu $2p_{3/2}$ spectrum due to KCN etching [Fig. 6(d)] we estimate the thickness of the native oxide layer (including all oxide phases) to be 20 Å using an inelastic mean free path of 8 Å for photoelectrons with $E_{kin} = 320$ eV.[52]

Our results show that the Cu^{2+} EPR signal found in thin films could only be detected after storage in air under ambient conditions for several months. On the other hand the degradation of solar cell devices occurs within few hours[4] or days.[5] Even after oxidation under humid conditions for 20 days no copper (II) oxide was detected on solar cell absorbers.[5] Further, the Cu^{2+} EPR signal vanishes after the CdS deposition (Fig. 4), as the ammonia in the chemical bath solution dissolves the $Cu(OH)_2$.[53] Hence, we conclude that the formation of $Cu(OH)_2$ associated with the observed Cu^{2+} EPR signal is not responsible for the degradation of solar cell devices consisting of p-type conducting $CuGaSe_2$ thin films. The degradation already takes place during the short term oxidation process before formation of $Cu(OH)_2$.

V. Conclusions

The native oxidation of $CuGaSe_2$ in air under ambient conditions was studied by EPR combined with PES. The EPR spectra of thin films presented here were made possible by means of a special peeling-off technique. Only after long term native oxidation for more than 4 months a Cu^{2+} signal was found in the thin-film samples. A similar Cu^{2+} signal was found in crystal and powder samples. By chemical treatments it was proved, that the Cu^{2+} signal is due to Cu^{2+} ions located in the surface/near-surface region. With help of photoemission spectra the Cu^{2+} EPR signal was attributed to a $Cu(OH)_2$ phase, which forms only after Ga_2O_3 and SeO_2 have already built up an oxide layer. Thermal reduction in vacuum reduces the $Cu(OH)_2$ phase likely to non paramagnetic Cu_2O. The activation energy for this reaction was determined to be $E_a = 0.29$ eV. From the different time scales for the growth of $Cu(OH)_2$ on thin films and the degradation of solar cells we exclude the Cu^{2+} EPR signal assigned to $Cu(OH)_2$ to be responsible for the degradation of solar cells.

Acknowledgements

The authors thank Hendrik Bluhm, Michael Hävecker, and Evgueni Kleimenov for providing us with their photoelectron-spectroscopy system at BESSY II. Further, the authors thank Rolf Follath for technical support at the BESSY II beamline U49/2 PGM1, Jörg Reichardt and Mirko Vogel for helping and performing XPS measurements in the laboratory, and Kai Petter and Christoph Boehme for support at the EPR setup. Thanks to Marin Rusu for thin film preparation, to Mario Birkholz for powder preparation, to Yvonne Tomm for growth of crystals, and to Norbert Blau, Iver Lauermann, and Xinyu Cao for chemical treatments. This work was supported by the Bundesministerium für Wirtschaft through its CCSVT-project (Contract No. 0329740B), which is gratefully acknowledged.

References

[1] M. Saad, H. Riazi-Nejad, E. Bucher, and M. Ch. Lux- Steiner, in *1st World Conference on Photovoltaic Energy Conversion* (IEEE, Hawaii, 1994), p. 214; M. Saad, H. Riazi, E. Bucher, and M. Ch. Lux-Steiner, Appl. Phys. A: Mater. Sci. Process. **62**, 181 (1996).

[2] D. L. Young, J. Keane, A. Duda, J. A. M. AabuShama, C. L. Perkins, M. Romero, and R. Noufi, Prog. Photovoltaics **11**, 535 (2003).

[3] M. A. Green, in *Solar Cells*, Prentice-Hall Series in Solid State Physical Electronics edited by Nick Holonyak, Jr. (Prentice-Hall, Englewood Cliffs, NJ, 1982).

[4] V. Nadenau, D. Hariskos, and H. W. Schock, in *14th European Photovoltaic Solar Energy Conference*, edited by H. Ossenbrink,

P. Helm, and H. Ehmann (Stephens & Associates, Barcelona, 1997), p. 1250.
[5] D. Hariskos, G. Bilger, D. Braunger, M. Ruckh, and H. W. Schock, Inst. Phys. Conf. Ser. **152** 707 (1997).
[6] H. J. von Bardeleben and R. D. Tomlinson, J. Phys. C **13**, L1097 (1980).
[7] J. M. Tchapkui-Niat, A. Goltzene, and C. Schwab, J. Phys. C **15**, 4671 (1982).
[8] Y. J. Hsu and H. L. Hwang, J. Appl. Phys. **66**, 5798 (1989).
[9] G. K. Padam, G. L. Malhotra, and S. K. Gupta, Sol. Energy Mater. **22**, 303 (1991).
[10] N. Nishikawa, I. Aksenov, T. Shinzato, T. Sakamoto, and K. Sato, Jpn. J. Appl. Phys., Part 2 **34**, L975 (1995).
[11] M. Birkholz, P. Kanschat, T. Weiss, M. Czerwensky, and K Lips, Phys. Rev. B **59**, 12268 (1999).
[12] M. Birkholz, P. Kanschat, T. Weiss, and K. Lips, Thin Solid Films **361**, 243 (2000).
[13] T. Nishi, G. A. Medvedkin, Y. Katsumata, K. Sato, and H. Miyake, Jpn. J. Appl. Phys. Part 1 **40**, 59 (2001); T. Nishi, Y. Katsumata, K. Sato, and H. Miyake, Sol. Energy Mater. Sol. Cells **67**, 273 (2001).
[14] G. A. Medvedkin, T. Nishi, Y. Katsumata, H. Miyake, and K. Sato, Sol. Energy Mater. Sol. Cells **75**, 135 (2003).
[15] I. H. Parker, J. Phys. C **4**, 2967 (1971).
[16] F. J. Owens, J. Appl. Phys. **53**, 368 (1982).
[17] S. K. Hoffmann, J. Goslar, and L. S. Szczepaniak, Phys. Rev. B **37**, 7331 (1988).
[18] G. Córdoba, M. Viniegra, J. L. G. Fierro, J. Padilla, and R. Arroyo, J. Solid State Chem. **138**, 1 (1998).
[19] A. Durán, J. M. Fernández Navarro, J. García Solé, and F. Agulló-López, J. Mater. Sci. **19**, 1468 (1984).
[20] B. Sreedhar, Ch. Sumalatha, and K. Kojima, J. Non-Cryst. Solids **192**, 203 (1995).
[21] H. Imagawa, Phys. Status Solidi **30**, 469 (1968).
[22] D. Fischer, N. Meyer, M. Kuczmik, M. Beck, A. Jäger-Waldau, and M. Ch. Lux-Steiner, Sol. Energy Mater. Sol. Cells **67**, 105 (2001).
[23] D. Fischer, T. Dylla, N. Meyer, M. E. Beck, A. Jäger-Waldau, and M. Ch. Lux-Steiner, Thin Solid Films **387**, 63 (2001).
[24] R. Würz, D. Fuertes Marrón, A. Meeder, A. Rumberg, S. M. Babu, Th. Schedel-Niedrig, U. Bloeck, P. Schubert Bischoff, and M. Ch. Lux-Steiner, Thin Solid Films **431**, 398 (2003); patent No. DE 102 47 735.3; international patent PCT/DE03/03371.
[25] K. Lips (private communication).
[26] D. Fischer, Ph.D. thesis, Free University of Berlin, 2000.
[27] Y. Hashimoto, N. Kohara, T. Negami, M. Nishitani, and T. Wada, Jpn. J. Appl. Phys., Part 1 **35**, 4760 (1996).
[28] L. C. Olsen, F. W. Addis, L. Huang, W. N. Shafarman, P. Eschbach, and G. J. Exarhos, *Conference Record of the 28th IEEE Photovoltaic Specialists Conference-2000*, Piscataway, NJ, 2000, p. 458.
[29] A. Kylner, J. Electrochem. Soc. **146**, 1816 (1999).
[30] A. Jasenek, U. Rau, V. Nadenau, and H. W. Schock, J. Appl. Phys. **87**, 594 (2000).
[31] S. D. Setzler, M. Moldovan, Zhonghai Yu, T. H. Myers, N. C. Giles, and L. E. Halliburton, Appl. Phys. Lett. **70**, 2274 (1997).
[32] A. Meeder, L. Weinhardt, R. Stresing, D. Fuertes Marrón, R. Würz, S. M. Babu, T. Schedel-Niedrig, M. Ch. Lux-Steiner, C. Heske and E. Umbach, J. Phys. Chem. Solids **64**, 1553 (2003).
[33] L. L. Kazmerski, O. Jamjoum, P. J. Ireland, and S. K. Deb, J. Vac. Sci. Technol. **19**, 467 (1981).
[34] L. Fiermans, R. Hoogewijs, and J. Vennik, Surf. Sci. **47**, 1 (1975).
[35] N. S. McIntyre and M. G. Cook, Anal. Chem. **47**, 2208 (1975).
[36] N. S. McIntyre, S. Sunder, D. W. Shoesmith, and F. W. Stanchell, J. Vac. Sci. Technol. **18**, 714 (1981).
[37] C. D. Wagner, W. M. Riggs, L. E. Davis, and J. F. Moulder, in *Handbook of X-Ray Photoelectron Spectroscopy*, edited by G. E. Muilenberg (Perkin Elmer, Eden Prairie, MN, 1978).
[38] D. Schmid, M. Ruckh, and H. W. Schock, Appl. Surf. Sci. **103**, 409 (1996).
[39] G. Leonhardt, A. Berndtsson, J. Hedman, M. Klasson, R. Nilsson, and C. Nordling, Phys. Status Solidi B **60**, 241 (1973).
[40] Although the Ga 3*d* peak after KCN etching is shifted by 0.2 eV to higher binding energy compared to that of the virgin film, the Ga $L_2M_{45}M_{45}$ Auger spectrum after KCN etching reveals, that the Ga_2O_3 phase has been completely removed by KCN.
[41] M. K. Bahl, R. L. Watson, and K. J. Irgolic, Anal. Chem. **51**, 466 (1979).
[42] D. Cahen, P. J. Ireland, L. L. Kazmerski, and F. A. Thiel, J. Appl. Phys. **57**, 4761 (1985).
[43] E. P. Domashevskaya, V. V. Gorbachev, V. A. Terekhov, V. M. Kashkarov, E. V. Panfilova, and A. V. Shchukarev, J. Electron Spectrosc. Relat. Phenom. **114-116**, 901 (2001).
[44] A. Zangwill, *Physics at Surfaces* (Cambridge University Press, Cambridge, 1983); G. A. Somorjai, *Chemistry in Two Dimensions: Surfaces* (Cornell University Press, Ithaca, NY, 1981).
[45] J. D. Cox, D. D. Wagman and V. A. Medvedev, in *CRC Handbook of Chemistry and Physics 2001-2002: A Ready-Reference Book of Chemical and Physical Data*, 82nd ed., edited by D. R. Lide (CRC, Boca Raton, FL, 2001).
[46] O. Knacke, O. Kubaschewski, and K. Hesselmann, *Thermochemical Properties of Inorganic Substances* (Springer, New York, 1991).
[47] H. Schmalzried, *Chemical Kinetics of Solids* (VCH, Weinheim, 1995), Chap. 6, p. 7.
[48] E. Cano, M. F. López, J. Simancas, and J. M. Bastidas, J. Electrochem. Soc. **148**, E26 (2001).
[49] Y. Z. Hu, R. Sharangpani, and S. P. Tay, J. Vac. Sci. Technol. A **18**, 2527 (2000).
[50] P. D. Kirsch and J. G. Ekerdt, J. Appl. Phys. **90**, 4256 (2001).
[51] Jian Li, G. Vizkelethy, P. Revesz, J. W. Mayer, L. J. Matienzo, F. Emmi, C. Ortega, and J. Siejka, Appl. Phys. Lett. **58**, 1344 (1991).
[52] S. Tanuma, C. J. Powell, and D. R. Penn, Surf. Interface Anal. **17**, 911 (1991).
[53] E. H. Erich Pietsch, *Gmelins Handbuch der anorganischen Chemie* (Verlag Chemie, Weinheim, 1958), Kupfer Teil B, System Nr. 60.